RESEARCH PAPER

Removal of Crystal Violet Dye from Aqueous Solution Using the Surface of Soot-Poly(o-toluidine) Nanocomposite Treated with Nitric Acid

Mohammed Adil Naji *, Hassan Sabih Jabr*

Department of Chemistry, College of Science, Al-Muthanna University, Samawah, Iraq

ARTICLE INFO

ABSTRACT

In our current research, Soot–Poly(O-Toluidine) nanocomposite (St–POT) were prepared from soot and *o*-toluidine via in situ oxidative polymerization under ultrasound field. Then, the surface properties of the nanocomposite, such as roughness and surface area, were improved using acid treatment with nitric acid. AFM and BET techniques supported this matter, as the surface area and roughness of the Soot–Poly(O-Toluidine) nanocomposite treated with nitric acid (St–POT@Ac) increased. Other techniques were also used to characterize the prepared nanocomposite, such as FT-IR, XRD, and FE-SEM. We have conducted a number of experiments and studies to reach the optimal conditions for removing crystal violet dye (CV), where the removal rate reached 99.1% at a time of 40 minutes and adsorbent weight of 0.1g at 25°C. Thermodynamic study indicated that the adsorption process is physisorption, exothermic, and spontaneous. The adsorption isotherm was fitted to the Freundlich equation, while the kinetic isotherm was fitted to the pseudo-second order equation.

INTRODUCTION

In recent years, interest in nanotechnology and the development of nanomaterials has surged due to its optical, mechanical, electrical, and chemical properties. Nanomaterials are involved in a number of fields, including biology, electronics, high-density magnetic recording media, chemistry, and sensors [1]. Nanocomposites are a class of nanomaterials that is composed of materials such as ceramic, metal, or polymers that have one or more nanoscale phases embedded in them. These can be produced by molecularly combining organic or inorganic components to provide new properties. It differs from ordinary composites due to its high surface-to-volume ratio [2]. The main advantage of this technology is that it can dispose of wastewater in a suitable period of time, in addition to its low cost, high stability, mechanical strength and high resistance which has led to great interest in its use for wastewater treatment [3].

Pyrogenic carbon materials such as activated carbon, charcoal and soot are strong adsorbents, making them suitable for adsorption. These nanoparticles are combined with polymers to achieve the synergistic effect and improve the conductivity of the polymeric nanocomposite [4]. One of the conducting polymers with the most potential for usage as effective adsorbents is poly aromatic amines, which have drawn a lot of interest recently due to their environmental

* *Corresponding Author Email: mohammed.adil.scic@mu.edu.iq*

stability, ease of synthesis, and low cost [5].

The presence of dyes in wastewater leads to significant damage to the surface water ecosystem and pollution of groundwater resources. The use of dyes has increased globally, and has moved from small industries to major industries, where they have been used in countless wide fields [6]. The leakage of these dyes into wastewater has become a serious matter in recent decades, as they have an impact on the aquatic environment with all its organisms, and on humans in particular, as they are considered among the factors that cause cancerous diseases, especially amino dye [7]. This risk arises from the possibility that these dyes will break down into dangerous amines and benzidine, which are well-known carcinogens that are easily released throughout the dyeing and manufacturing processes [8]. This necessitates rigorous scientific attention and the development of safer alternatives to mitigate the concerning. In this research, a nanocomposite of poly(o-toluidine) (see Fig. 1) and soot was prepared and used as an adsorption surface to remove CV dye from its aqueous solutions.

MATERIALS AND METHODS
Materials

All chemicals employed in this study were of high purity (AR grade), which includes Ammonium sulfate (98%), O-toluidine (99%), and nitric acid (69%) were purchased from Sigma-Aldrich. While sodium hydroxide (97%) and hydrochloric acid (38%) were purchased from BDH. The soot was collected from a paraffin candles.

Preparation of St–POT nanocomposite

By using oxidative polymerization, the St-POT nanocomposite was prepared, with a 1:5 mixing ratio between the soot and o-toluidine monomer. In an ultrasonic water bath, 1.0 g of soot was added to a solution containing 0.05 moles each of o-toluidine monomer and HCl (1M). The prepared mixture was then put in an ice bath, and addition of ammonium persulfate solution (0.05 mol of APS dissolved in 100 ml of 1.0 M HCl) was made dropwise. After 5 hours of magnetic stirring in an ice bath, the mixed solution was left to sit at room temperature for 24 hours to allow the polymerization process to complete. Ultimately, a centrifuge was used to separate the mixture, and the precipitate was repeatedly washed with deionized water and dried at 60 °C [10][11].

Treatment St–POT with nitric acid

5g of the St–POT added to a beaker containing 100 ml of nitric acid 10% and stirred using a magnetic stirrer at 40°C for two hours, then filtered, washed with deionized water, and dried at 60 °C [12]. Give him the symbol St–POT@Ac.

Adsorption Experiment

The effect of different parameters on the adsorption of the CV dye was studied by batch adsorption experiments. By changing one
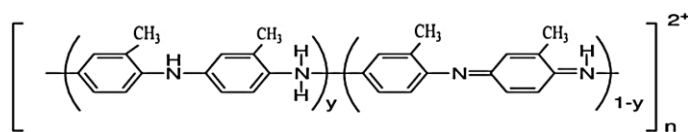

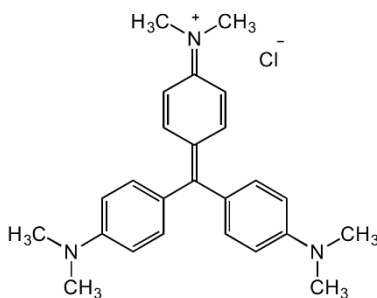Fig. 1. Chemical Structures of poly(o-toluidine) [9].

Fig. 2. Chemical Structures of crystal violet dye [15].

of the study's parameters while keeping the others constant, the effect of the adsorbent weight, contact time, temperature, pH, and dye concentration on the adsorption performance was studied. To prepare a 1000 ppm stock solution of CV dye, 1.0 gm of dye was dissolved in 1000 ml of deionized water. The chemical structure of CV dye are shown in Fig. 2. Prepare a series of solutions of the dye with concentrations ranging from (5 - 25) ppm by diluting the stock solution. 10 ml of each concentration were placed in a conical flask. Each flask contains a fixed weight of adsorbent (0.01 g). The flasks were stirred in a shaking water bath at 125 rpm and 25°C until equilibrium time. After that, the solutions concentration of the two dye were measured by using a UV-Vis spectrophotometer (PerkinElmer Lambda 35, Singapore) set at 584 nm. The removal percentage (%R) and the quantity of CV dye absorbed on the surface were calculated using equations 1 and 2

respectively [13,14].

$$q_e = \frac{(C_o - C_e)\,V}{m} \qquad (1)$$

$$\%R = \frac{(C_o - C_e)}{C_o} \times 100 \qquad (2)$$

Where qe is the amount of CV dye adsorbed at equilibrium time (g/mg), Co and Ce are the initial and equilibrium concentrations of the CV dye. While, V and m are the volume of the solution and weight of the adsorbent.

RESULTS AND DISCUSSION
Characterization

The prepared materials were analyzed by FT-IR technology and the results are shown in Fig. 3. The soot spectrum in Fig. 3 (a) shows peaks at 1523 cm^{-1} that belong to the aromatic C=C stretching vibration, while the peak at 1749 cm^{-1} belongs to the C=O of the carboxyl group. The broad peak
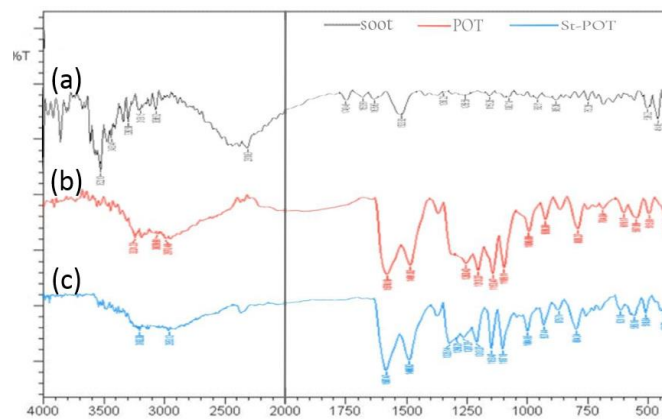

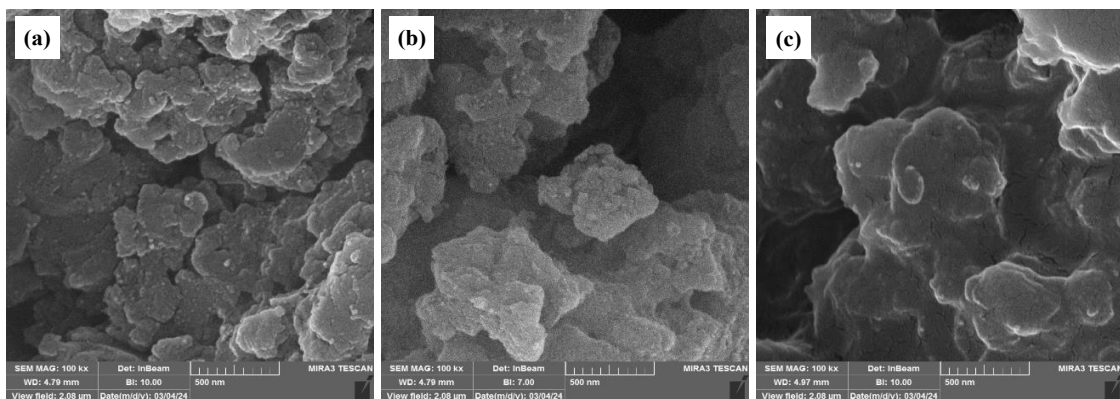Fig. 3. FT–IR spectrum of (a) Soot, (b) POT, and (c) St–POT@Ac nanocomposite

Fig. 4. FE-SEM images of (a) POT, (b) St-POT, and (c) St–POT@Ac.

in the range 3292-3522 cm^{-1} is related to O-H stretching [16].

Fig. 3 (b, c) show the spectrum of POT and St–POT@Ac, respectively. We note that there is similarity in the peaks, but there are shifts and differences in peak intensity. The two peaks that appear at 1491 cm^{-1} and 1578 cm^{-1} in the POT spectrum belong to the C=C of the benzenoid ring and the quinoid ring, respectively. These two peaks are shifted in the St–POT@Ac, where they appear at 1496 cm^{-1} and 1587 cm^{-1}, this occurs as a result of π-π stacking, which is due to the interference of π electrons of the aromatic rings in the POT and the soot. There is also a shift at the peak from 3221 cm^{-1} to 3192 cm^{-1} that indicates the N-H stretching vibration as a result of hydrogen bonding between H and the functional groups on the soot surface [17].
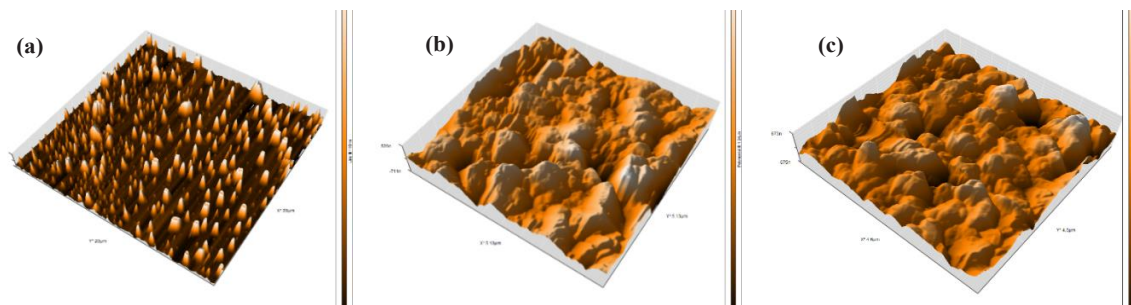

Fig. 5. The AFM images of (a) POT, (b) St–POT, and (c) St–POT@Ac

Table 1. Roughness parameters of the prepared material particles

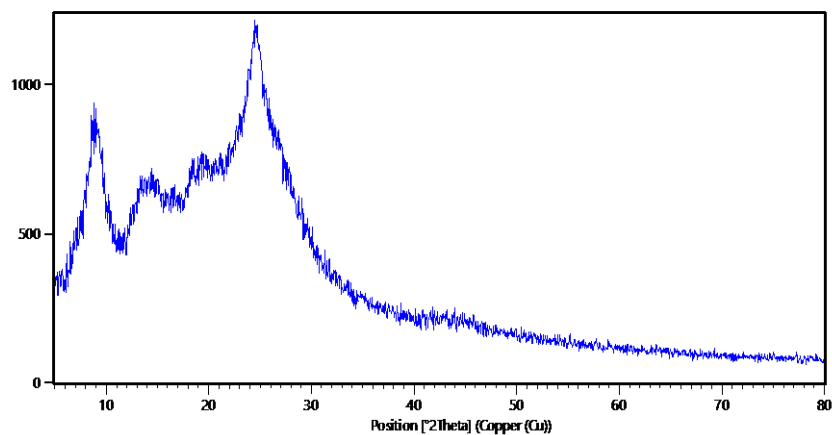| Materials	Density Particles/mm^2	Roughness Average Ra (nm)	R$_{SK}$	R$_{KU}$
POT	3068799	165.1	0.46040	2.722
St-POT	6157565	69.97	-0.04885	3.729
St-POT@Ac	5723860	78.30	-0.09783	4.282

Fig. 6. XRD patterns of St–POT nanocomposites

Fig. 4 shows scanning electron microscopic (FE-SEM) images of the prepared materials. From Fig. 4(b) it clearly indicates that the soot particles spread on the polymer surface uniformly and have a rough surface. Fig. 4(c) indicates the presence of cracks in the surface as a result of treatment with nitric acid, and this leads to an increase in the surface area.

Fig. 5 shows AFM 3D images to study surface topography and roughness. It is clear that the surface of St–POT@Ac is rough and contains homogeneously distributed porosity, and the highest height it reaches is 673 nm. The roughness parameters listed in Table 1. indicate that the surface of St–POT@Ac is rougher than of St–POT, and this leads to an increase in the surface area, as was confirmed by BET analysis. The presence of the negative value of RSK in the nanocomposites indicates the presence of a greater number of valleys compared to the peaks, and the spiky nature of the surface (R_{ku}>3) [18].

The crystal structure of the St–POT@Ac nanocomposite was determined by X-ray diffraction (XRD) technique. The XRD results showed that the diffraction pattern of the nanocomposite did not contain distinct sharp peaks, as shown in Fig. 6. Four broad peaks were observed at 2θ = 8.83°, 14.11°, 19.41°, and 24.59°. The absence of sharp peaks and the presence of broad peaks indicate that the St–POT@Ac nanocomposite exists in an amorphous structure. Using the Scherer equation (Equation 3), the crystal size was calculated and found to be 11.23nm [19].

$$D = \frac{K\lambda}{\beta \cos\theta} \qquad (3)$$

Where: D: average crystalline size. K: is the shape factor whose value is 0.9. λ: is the wavelength of the incident X-ray (0.15406 nm). β; is FWHM (full width at half maximum). θ: is diffraction angle.

BET analysis was performed to study the surface area. Fig. 7 shows the adsorption and desorption of nitrogen on the prepared surfaces, and when matching it according to the IUPAC classification, it is clear that the isotherm is of type IV, which indicates multilayer adsorption and capillary condensation of a porous nanocomposite. While
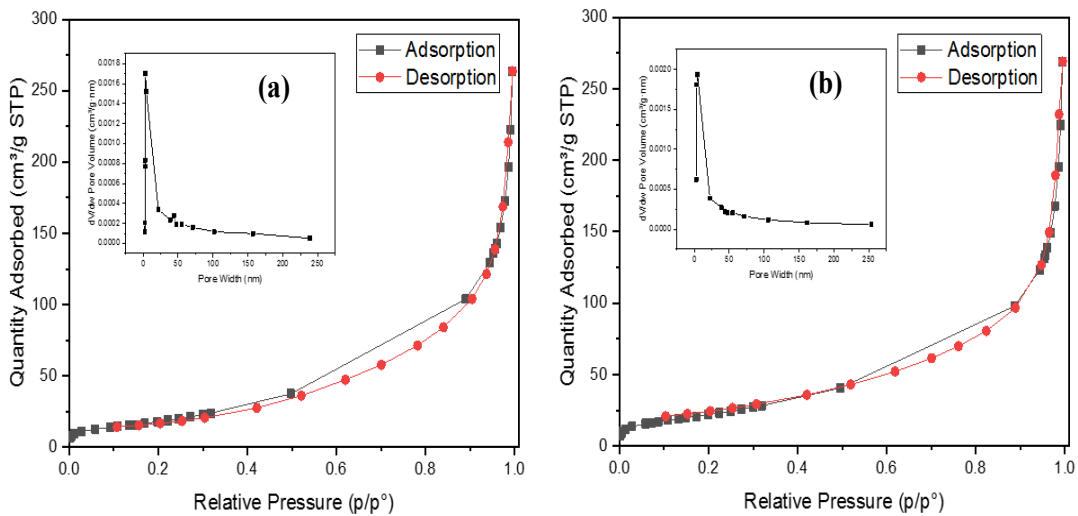

Fig. 7. BET isotherms of Nitrogen adsorption- desorption with BJH pore size distribution curve of (a) St–POT and (b) St–POT@Ac nanocomposites

Table 2. Surface area, pore volume, and average diameter of prepared nanocomposites

Materials	Surface area (m^2/g)	Total pore Volume (cm^3/g)	Average pore diameter (nm)
St-POT	73.32	0.0254	9.205
St-POT@Ac	86.53	0.0297	11.386

type H3 hysteresis loops, which indicate narrow sheet-like pores, have been described [20]. The analysis showed that the surface area of the St–POT@Ac is more than St–POT. The surface area, pore size, and average diameter of the prepared material were also known and are listed in Table 2.

Study the effect of the Contact Time and Adsorption Kinetics

This study is conducted at 25°C using a fixed adsorbent (St–POT@Ac) weight of 0.01g and the dye concentration of 25 ppm. Different time periods ranging (10-90) minutes are taken to determine the optimal equilibrium time for removing CV dye from the aqueous solution and study the adsorption kinetics. The volume of dye solution were kept constant at 10 ml for all experiments. The removal of CV dye by a composite surface is shown in Fig. 8, which reaches equilibrium in 40 minutes. The removal
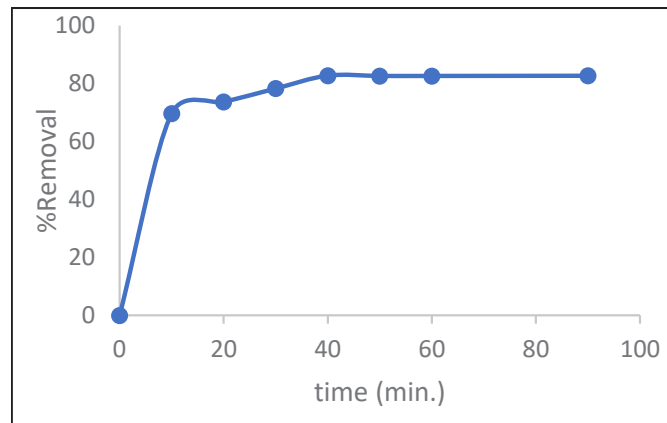

Fig. 8. Effect of equilibrium time
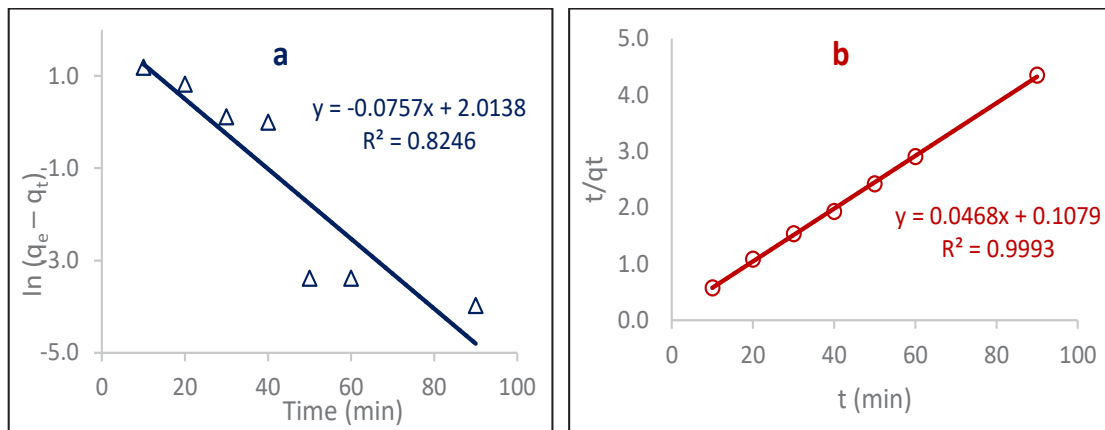
Fig. 9. The kinetics graphs models: (a) pseudo-first-order model and (b) pseudo-second-order model

Table 3. Kinetic data of adsorption CV dye onto St–POT@Ac nanocomposite.

q_e (exp.) (mg/g)	pseudo-first-order model			pseudo-second-order model		
	K_1 (min^{-1})	q_e (cal.) (mg/g)	R^2	K_2 (mg/g.min)	q_e (cal.) (mg/g)	R^2
20.69	0.0757	7.49	0.8246	0.0203	21.37	0.9993

of dye increases significantly in the first minutes due to the amount of vacant active sites on the surface. Thereafter, the adsorption rate decreases as the number of dye molecules occupying these sites increases. Finally, equilibration is achieved when all available sites are occupied [21].

After that, the adsorption kinetics of CV dye on the St–POT@Ac surface were studied using pseudo-first-order and pseudo-second-order Lagergren models. The Langergren equation is an important equation because it describes the rate of adsorption. The models are expressed by the following equations:

The pseudo-first-order model:

$$\ln(q_e - q_t) = \ln q_e - K_1 t \tag{4}$$

The pseudo-second-order model:

$$\frac{t}{q_t} = \frac{1}{K_2 q_e^2} + \frac{1}{q_e} t \tag{5}$$

Where qe and qt are the amount of dye adsorbed at equilibrium and at a certain time (t), respectively (mg/g), K_1 is the pseudo-first-order rate constant (min^{-1}), K_2 is the pseudo-second-order rate constant (mg.g^{-1}.min^{-1}). The linear form of these models is shown in Fig. 9 (a, b). Based on the calculations of the correlation coefficients and kinetic constants for the two models provided in Table 3., the correlation coefficient for the pseudo-second-order model is somewhat greater than the correlation coefficient for the pseudo-first-order model. This leads us to conclude that
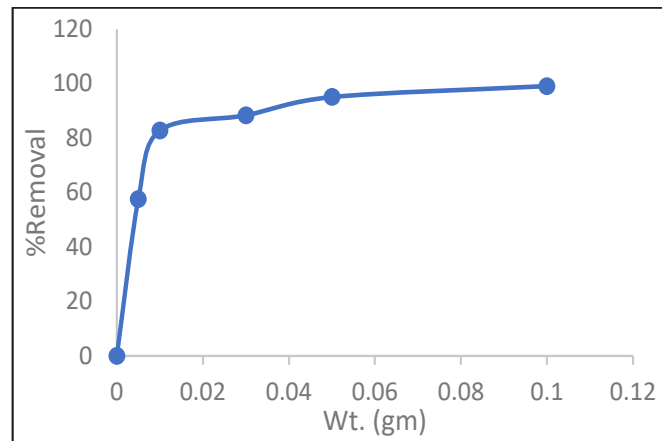

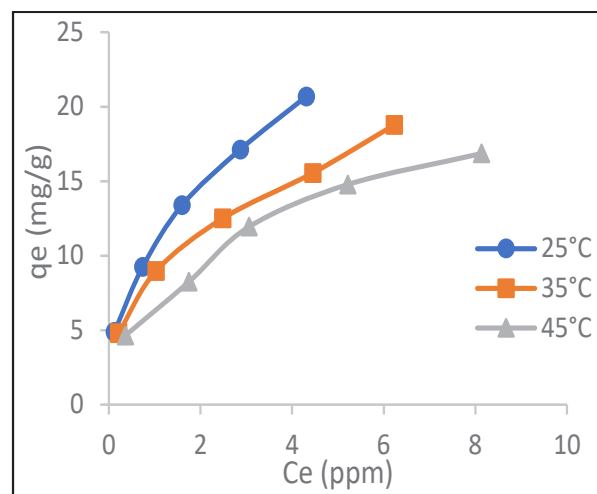Fig. 10. Effect of adsorbent weight

Fig. 11. Effect of the temperature on the adsorption process

the adsorption process of the CV dye on the St–POT@Ac surface follows the pseudo-second order [22,23].

Study the effect of adsorbent weight

The effect of the adsorbent's weight on the adsorption process was studied at 25°C. Different weights were taken from the adsorbent (0.005, 0.01, 0.03, 0.05, and 0.1) gm and dye volume and concentration (10 ml, 25 ppm) and equilibrium time is 40 minutes. The results showed that as the weight of the adsorbent increased, the rate of adsorption of the dye increased. Fig. 10 shows the effect of adsorbent weight on the adsorption. This can be attributed to both the increase in the adsorbent surface area and the number of active sites on the surface. As a result, the surface efficacy increases and the adsorption percentage increase as well [24].

Study the effect of the temperature on the adsorption process

Three different temperatures (25, 35, and 45) °C as well as a constant adsorbent weight of 0.01 g and a constant dye solution concentration and volume of (25 ppm, 10 ml) were used to Study the effect of temperature on adsorption. The study proved that the process is exothermic, as Fig. 11 illustrates, adsorption efficiency decreases with temperature. This may be explained that when
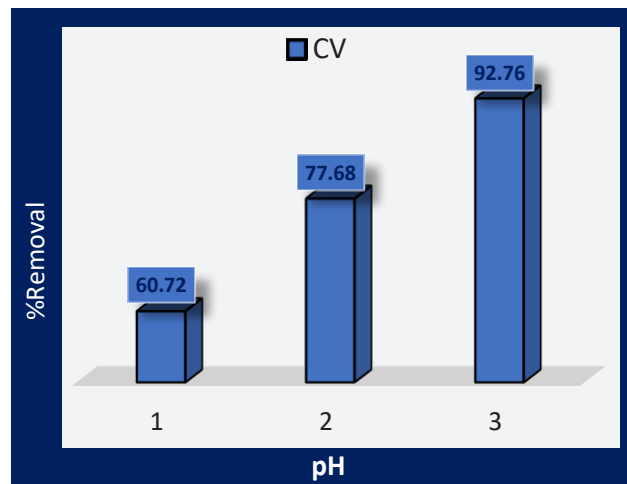

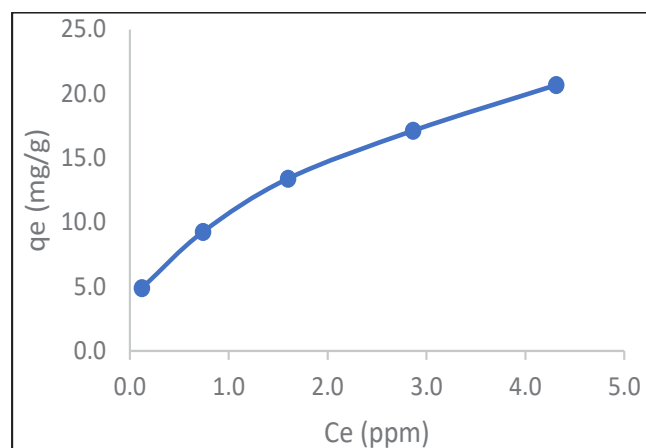Fig. 12. the effect of pH on the adsorption of CV dye

Fig. 13. Adsorption isotherm for CV dye with adsorbent.

temperature increases, the kinetic energy of the particles also increases, increasing the likelihood that the adsorbed particles will escape the adsorbent's surface [25].

Study the effect of pH

To study the effect of pH on CV dye adsorption, a constant volume and concentration (10 ml, 25 ppm) of the solution of the dye was taken, and its pH was set at (3, 7, and 10). (0.1N) of NaOH and HCl were used to control the pH. The temperature 25°C, the equilibrium time of 40 minutes, and the weight of the adsorbent (0.01 gram) were all predetermined. From Fig. 12, we notice that the percentage of removal of the CV dye increases when the medium is basic, while it decreases when the medium is acidic. The reason is that the basic medium causes deprotonation, which increases the negative charge on the surface and leads to an increase in the electrostatic attraction with the positively charged dye [26].

Study of Adsorption Isotherms

In the adsorption process, isotherm study is necessary to clarify the relationship between the amount of substance adsorbed on the surface (q_e) and the concentration of the substance in the liquid phase (C_e) while maintaining a constant

temperature (T) as Fig. 12. This study provides invaluable information into the adsorption process, allowing analysis and prediction of the adsorption behavior of different systems. Isotherm analysis was performed by applying the Langmuir and Freundlich equations to the experimental data as follows [28]:

The Langmuir equation: $\frac{C_e}{q_e} = \frac{1}{Q_{max} \; K_L} + \frac{C_e}{Q_{max}}$

The Freundlich equations: $\log q_e = \log K_f +$

$\frac{1}{n} \log C_e$ \hfill (7)

Where C_e is equilibrium concentration of dye in solution (mg/L), qe is the amount of dye adsorbed (mg/g) at equilibrium state, Q_{max} is the maximum adsorption capacity (mg/g), K_L is the Langmuir constant which is related to the energy of adsorption (L mg^{-1}), K_f and n are Freundlich constant and intensity of adsorption, respectively. (C_e/qe) versus Ce and log qe versus log C_e are plotted. The first drawing, which represents the Langmuir equation, showed a straight line with a slope ($1/Q_{max}$) and an intercept ($1/Q_{max}K_L$), while the second drawing, which represented
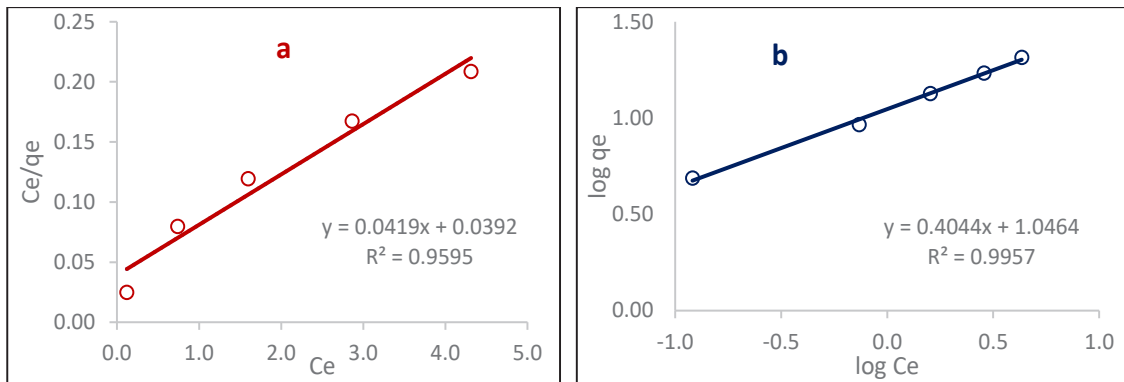

Fig. 14. (a, b) Langmuir and Freundlich models, respectively.

Table 4. Includes data for isotherm models used in the study of AR dye adsorption.

Langmuir			Freundlich		
q$_{max}$(mg/g)	K$_L$(L/mg)	R^2	1/n	K$_f$ (mg/g)(L/mg)$^{1/n}$	R^2
23.866	1.069	0.9595	0.4044	11.128	0.9957

the Freundlich equation, showed a slope (1/n) and an intercept (logK$_f$). Adsorption isotherm parameters were extracted from Fig. 13 (a, b) and listed in Table 4. When comparing the correlation coefficient (R^2) for both the Langmuir isotherm and the Freundlich isotherm, it was found that the R^2 value for the Freundlich equation was higher than the R^2 value for the Langmuir equation. This indicates that the Freundlich equation is more suitable to describe the adsorption process of CV dye from their aqueous solution on the surface of St–POT@Ac and this indicates that the adsorption process is multilayer [29].

Thermodynamic study

The thermodynamic functions of the adsorption of CV dye on the surface of St–POT@ Ac were studied in a temperature range of (25, 35, 45) °C. This study included calculating the Gibbs free energy change (ΔG°), entropy change (ΔS°), and enthalpy change (ΔH°). These functions are considered essential for understanding the adsorption process, as they provide information about the bond strengths between the adsorbent and the adsorbent, whether physical or chemical, the nature of the organization of the dye molecules on the surface of St–POT@Ac, and knowing the direction of the reaction, whether spontaneous or non-spontaneous. ΔG°, ΔS° and ΔH° were calculated using the following equations [30]:

$$\Delta G° = -RT \ln K_e \qquad (8)$$

$$\Delta G° = \Delta H° - T\Delta S° \qquad (9)$$

Where R is the universal gas constant (8.314 J.mol^{-1}.K^{-1}), T is the absolute temperature (in Kelvin), and K$_e$ is the equilibrium constant, which can be calculated from the following equation:

$$K_e = \frac{q_e \, m}{C_e \, V} \qquad (10)$$

From equations (5) and (6), gives the integrated form of the Van't Hoff equation:

$$\ln K = \frac{\Delta S°}{R} - \frac{\Delta H°}{RT} \qquad (11)$$
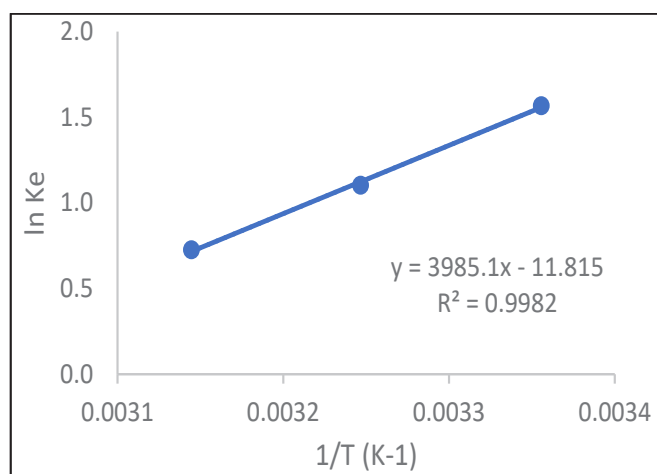
Fig. 15. Van't Hoff plots for the adsorption of CV dye onto St–POT@Ac surface

Table 5. Includes values of the equilibrium constant (ke) and thermodynamic parameters of adsorption the CV dye onto St–POT@Ac

Temperature (K)	K$_e$	ln K$_e$	ΔG° KJ.mol^{-1}	ΔH° KJ.mol^{-1}	ΔS° J.K^{-1}.mol^{-1}
298	4.80	1.57	-3.88	-33.13	-98.23
308	3.01	1.10	-2.82	-33.13	-98.23
318	2.07	0.73	-1.92	-33.13	-98.23

ln(K$_e$) was plotted against 1/T, as shown in Fig. 14. From this plots, (-ΔH°/R) and (ΔS°/R) were calculated, which represent the slope and intercept, respectively. Table 5 shows the values of the thermodynamic functions for the adsorption process of CV dye on the surface of St–POT@Ac. The following can be concluded from these values: A negative value of the free energy (ΔG°) indicates that the adsorption process is spontaneous, and a negative value of the enthalpy (ΔH°) indicates that the adsorption process is exothermic, as the adsorption process decreases with increasing temperature, due to separation and destruction of the weak bonds between the active sites on the surface of St–POT@Ac and the dye molecules. This indicates that the adsorption is physical [31].

CONCLUSION

Through FT-IR, XRD, AFM, and FE-SEM techniques, the success of preparing the nanocomposite was determined, and its surface properties were successfully improved using nitric acid. This result appeared on the removal of crystal violet dye from its aqueous solutions, and the optimum conditions were reached, where the removal reached 99%. We conclude from this that the nanocomposite treated with nitric acid is a good adsorbent surface.

CONFLICT OF INTEREST

The authors declare that there is no conflict of interests regarding the publication of this manuscript.

REFERENCES

1. Nguyen NPU, Dang NT, Doan L, Nguyen TTH. Synthesis of Silver Nanoparticles: From Conventional to 'Modern' Methods—A Review. Processes. 2023;11(9):2617.
2. Dghoughi A, Raji M, Nekhlaoui S, Essabir H, Bouhfid R, Qaiss Aek. Introduction of Nanomaterials and Polymer Nanocomposites. Smart Nanomaterials Technology: Springer Nature Singapore; 2023. p. 1-17.
3. Aragaw TA, Bogale FM, Aragaw BA. Iron-based nanoparticles in wastewater treatment: A review on synthesis methods, applications, and removal mechanisms. Journal of Saudi Chemical Society. 2021;25(8):101280.
4. Xiao F, Pignatello JJ. π$^+$–π Interactions between (Hetero) aromatic Amine Cations and the Graphitic Surfaces of Pyrogenic Carbonaceous Materials. Environmental Science and Technology. 2015;49(2):906-914.
5. Zare EN, Motahari A, Sillanpää M. Nanoadsorbents based on conducting polymer nanocomposites with main focus on polyaniline and its derivatives for removal of heavy metal ions/dyes: A review. Environ Res. 2018;162:173-195.
6. Uddin F. Environmental hazard in textile dyeing wastewater from local textile industry. Cellulose. 2021;28(17):10715-10739.
7. Richa, Roy Choudhury A. Synthesis of a novel gellan-pullulan nanogel and its application in adsorption of cationic dye from aqueous medium. Carbohydr Polym. 2020;227:115291.
8. Pielesz A, Baranowska I, Rybak A, Włochowicz A. Detection and Determination of Aromatic Amines as Products of Reductive Splitting from Selected Azo Dyes. Ecotoxicology and Environmental Safety. 2002;53(1):42-47.
9. Kovacic P, Khoury I, Elsenbaumer RL. Electrical conductivity of doped poly(1-methyl 2,5-pyrrolylene). Synthetic Metals. 1983;6:31-38.
10. Islam S, Sehrawat P, Khan H, Hashmi SA, Zulfequar M. Poly(o-toluidine)/multiwalled carbon nanotube-based nanocomposites: An efficient electrode material for supercapacitors. Journal of Materials Research. 2021;36(17):3472-3483.
11. Ghosh T, Ghosh R, Basak U, Majumdar S, Ball R, Mandal D, et al. Candle soot derived carbon nanodot/polyaniline hybrid materials through controlled grafting of polyaniline chains for supercapacitors. Journal of Materials Chemistry A. 2018;6(15):6476-6492.
12. Taloub N, Liu L, Du Y, Rahoui N, Huang Y. Surface modification of PIPD fiber using nitric acid treatment. Surface and Coatings Technology. 2018;334:312-318.
13. Tan IAW, Ahmad AL, Hameed BH. Adsorption of basic dye on high-surface-area activated carbon prepared from coconut husk: Equilibrium, kinetic and thermodynamic studies. J Hazard Mater. 2008;154(1-3):337-346.
14. Arami M, Limaee NY, Mahmoodi NM, Tabrizi NS. Removal of dyes from colored textile wastewater by orange peel adsorbent: Equilibrium and kinetic studies. Journal of Colloid and Interface Science. 2005;288(2):371-376.
15. Fekri MH, Mohamareh SI, Hosseini M, Mehr MR. Modification of Activated Carbon (Prepared From Flaxseed) With Fe$_3$O$_4$, Its Application As Adsorbent And Antibacterial. Research Square Platform LLC; 2021.
16. Salam Hassan Y. Adsorption study of Activated soot and its application as an adsorbent surface for removal of Alizarine Red S from aqueous Solution. Muthanna Journal of Pure Science. 2022;9(2):1-10.
17. Vargas LR, Poli AKDS, Dutra RdCL, De Souza CB, Baldan MR, Gonçalves ES. Formation of Composite Polyaniline and Graphene Oxide by Physical Mixture Method. Journal of Aerospace Technology and Management. 2017;9(1):29-38.
18. Tayebi N, Polycarpou AA. Modeling the effect of skewness and kurtosis on the static friction coefficient of rough surfaces. Tribology International. 2004;37(6):491-505.
19. Fatimah S, Ragadhita R, Husaeni DFA, Nandiyanto ABD. How to Calculate Crystallite Size from X-Ray Diffraction (XRD) using Scherrer Method. ASEAN Journal of Science and Engineering. 2021;2(1):65-76.
20. Sing KSW. Reporting physisorption data for gas/solid systems with special reference to the determination of surface area and porosity (Recommendations 1984). Pure and Applied Chemistry. 1985;57(4):603-619.
21. Oviedo LR, Oviedo VR, Dalla Nora LD, da Silva WL. Adsorption of organic dyes onto nanozeolites: A machine learning study. Sep Purif Technol. 2023;315:123712.
22. Revellame ED, Fortela DL, Sharp W, Hernandez R, Zappi ME. Adsorption kinetic modeling using pseudo-first order and pseudo-second order rate laws: A review. Cleaner Engineering and Technology. 2020;1:100032.
23. Ho YS, McKay G. Pseudo-second order model for sorption processes. Process Biochem. 1999;34(5):451-465.

24. Akhyar, Hesti M, Fauzi D, Sri M, Abrar M. Effectivity of dolomite adsorbent in purification of mn and cu from acid mine drainage. International Journal of Social Science, Educational, Economics, Agriculture Research and Technology (IJSET). 2023;2(6):86-96.

25. Abumelha HM, Alzahrani SO, Alrefaee SH, Al-bonayan AM, Alkhatib F, Saad FA, et al. Evaluation of tetracycline removal by magnetic metal organic framework from aqueous solutions: Adsorption isotherm, kinetics, thermodynamics, and Box-Behnken design optimization. Journal of Saudi Chemical Society. 2023;27(5):101706.

26. Aldegs Y, Elbarghouthi M, Elsheikh A, Walker G. Effect of solution pH, ionic strength, and temperature on adsorption behavior of reactive dyes on activated carbon. Dyes and Pigments. 2008;77(1):16-23.

27. Giles CH, Smith D, Huitson A. A general treatment and classification of the solute adsorption isotherm. I. Theoretical. Journal of Colloid and Interface Science. 1974;47(3):755-765.

28. Rajahmundry GK, Garlapati C, Kumar PS, Alwi RS, Vo D-VN. Statistical analysis of adsorption isotherm models and its appropriate selection. Chemosphere. 2021;276:130176.

29. Mittal A, Kurup L, Mittal J. Freundlich and Langmuir adsorption isotherms and kinetics for the removal of Tartrazine from aqueous solutions using hen feathers. J Hazard Mater. 2007;146(1-2):243-248.

30. Zghal S, Jedidi I, Cretin M, Cerneaux S, Abdelmouleh M. Adsorptive Removal of Rhodamine B Dye Using Carbon Graphite/CNT Composites as Adsorbents: Kinetics, Isotherms and Thermodynamic Study. Materials. 2023;16(3):1015.

31. Al-Johani H, Salam MA. Kinetics and thermodynamic study of aniline adsorption by multi-walled carbon nanotubes from aqueous solution. Journal of Colloid and Interface Science. 2011;360(2):760-767.